Electronic Supplementary Material (ESI) for Journal of Materials Chemistry C.


*Electronic Supporting Information (ESI)*

# Reversibly Thermochromic Bismuth–Organic Materials with Tunable Optical Gaps

**Guoxian Zhang,[†] Julian. M. W. Chan*[†]**

[†]Department of Chemistry and Biomolecular Sciences,
University of Ottawa, 10 Marie Curie Pvt.
Ottawa, Ontario, K1N 6N5, Canada
*E-mail: julian.chan@uottawa.ca
Group website: julianchangroup.com

## NMR spectra of MOF precursors synthesized using literature procedures:

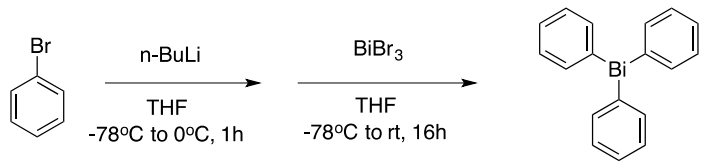


**Scheme S1.** Synthesis of triphenylbismuth.[1]

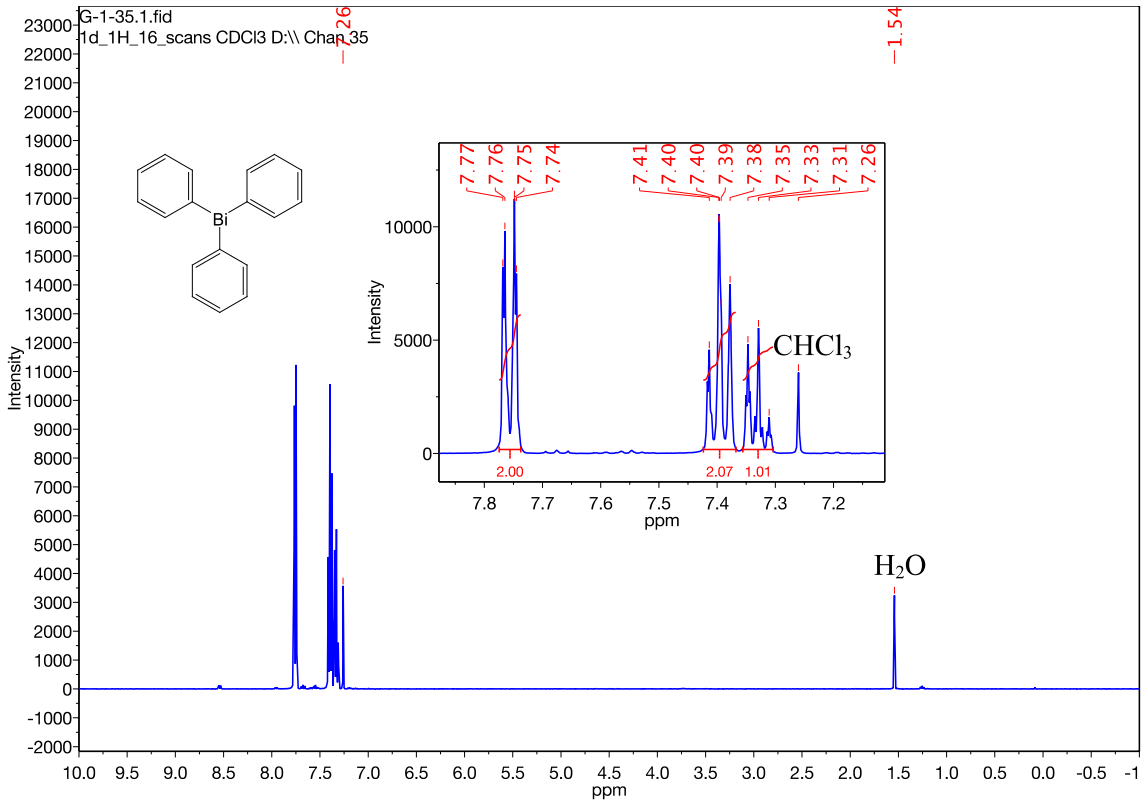


**Figure S1.** $^1$H NMR spectrum of triphenylbismuth in $CDCl_3$.

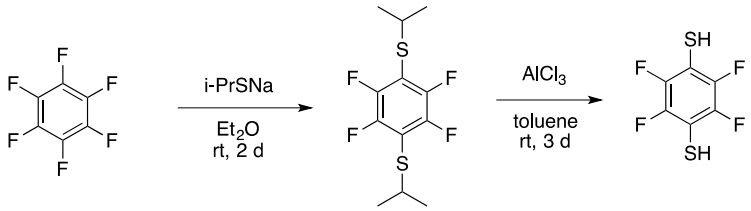


**Scheme S2.** Synthesis of the **Bi-OM-4** precursor dithiol.[2]

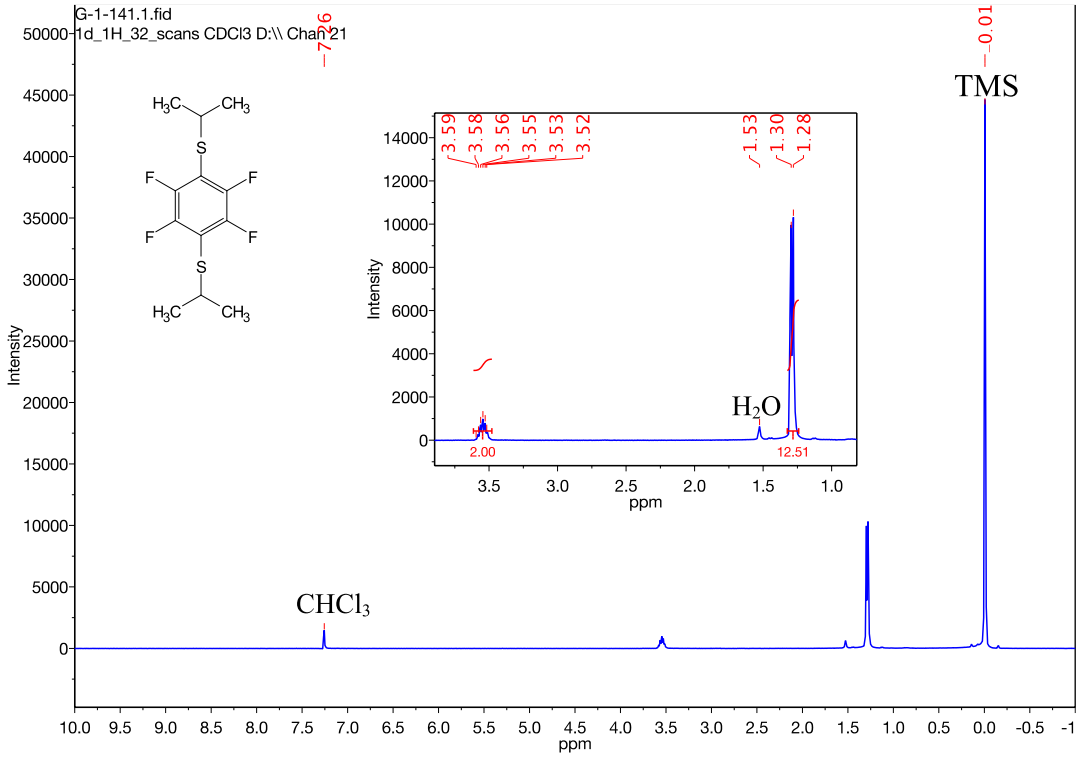


**Figure S2.** $^{1}$H NMR spectrum of 1,4-bis(isopropylthio)-2,3,5,6-tetrafluorobenzene in $CDCl_3$.

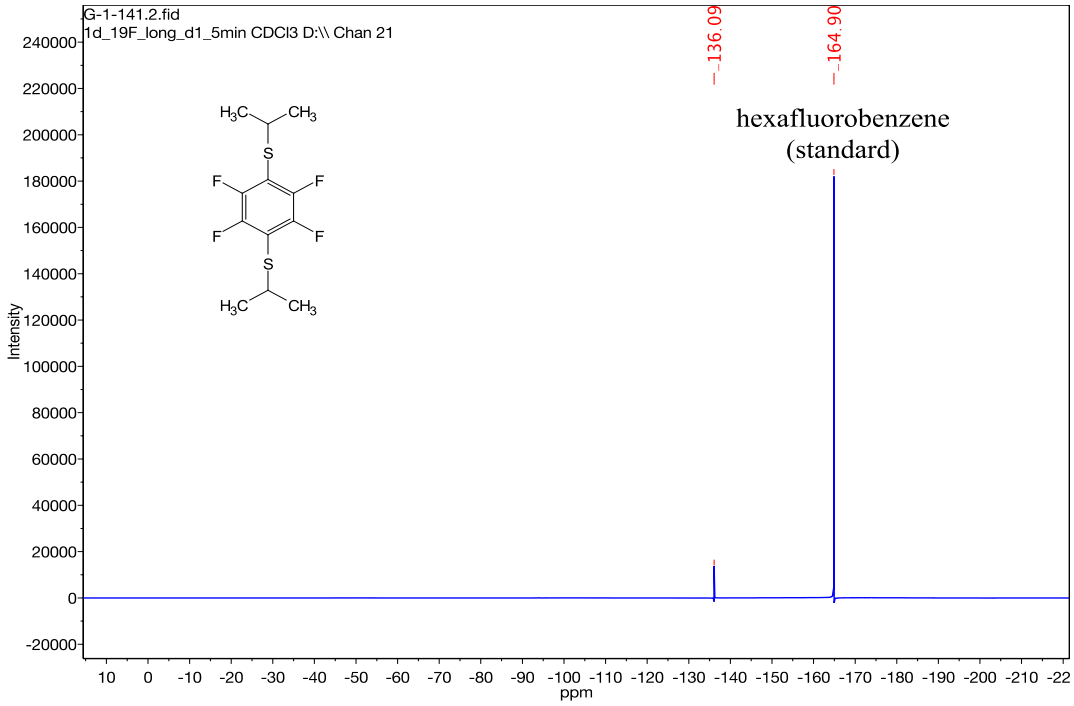


**Figure S3.** $^{19}$F NMR spectrum of 1,4-bis(isopropylthio)-2,3,5,6-tetrafluorobenzene in $CDCl_3$.

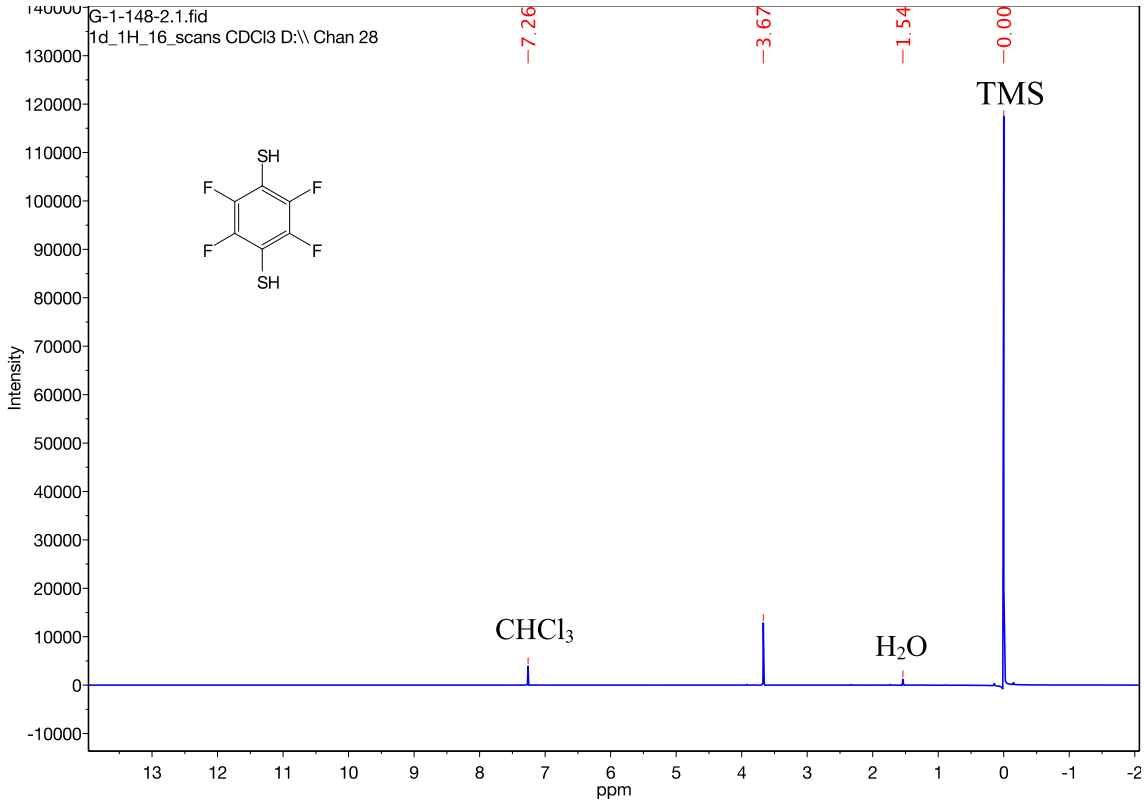


**Figure S4.** $^{1}$H NMR spectrum of 1,2,4,5-tetrafluorobenzene-1,4-dithiol in $CDCl_3$.

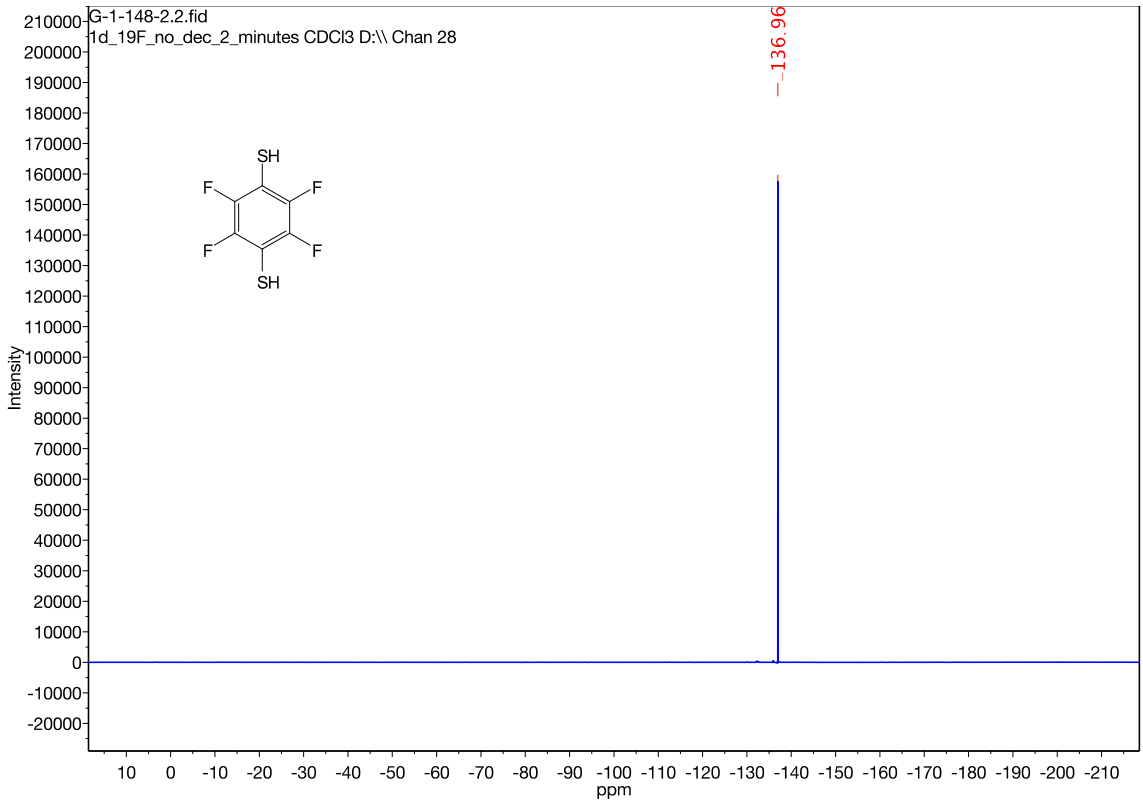


**Figure S5.** $^{19}$F NMR spectrum of 1,2,4,5-tetrafluorobenzene-1,4-dithiol in $CDCl_3$.

(All NMR characterization data were compared against literature values and found to be in good agreement.)

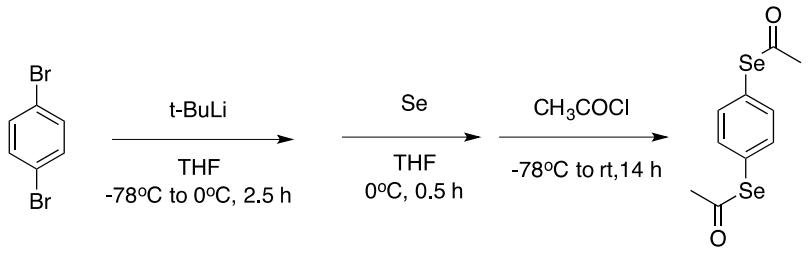


**Scheme S3.** Synthesis of 1,4-(diacetylseleno)benzene.[3]

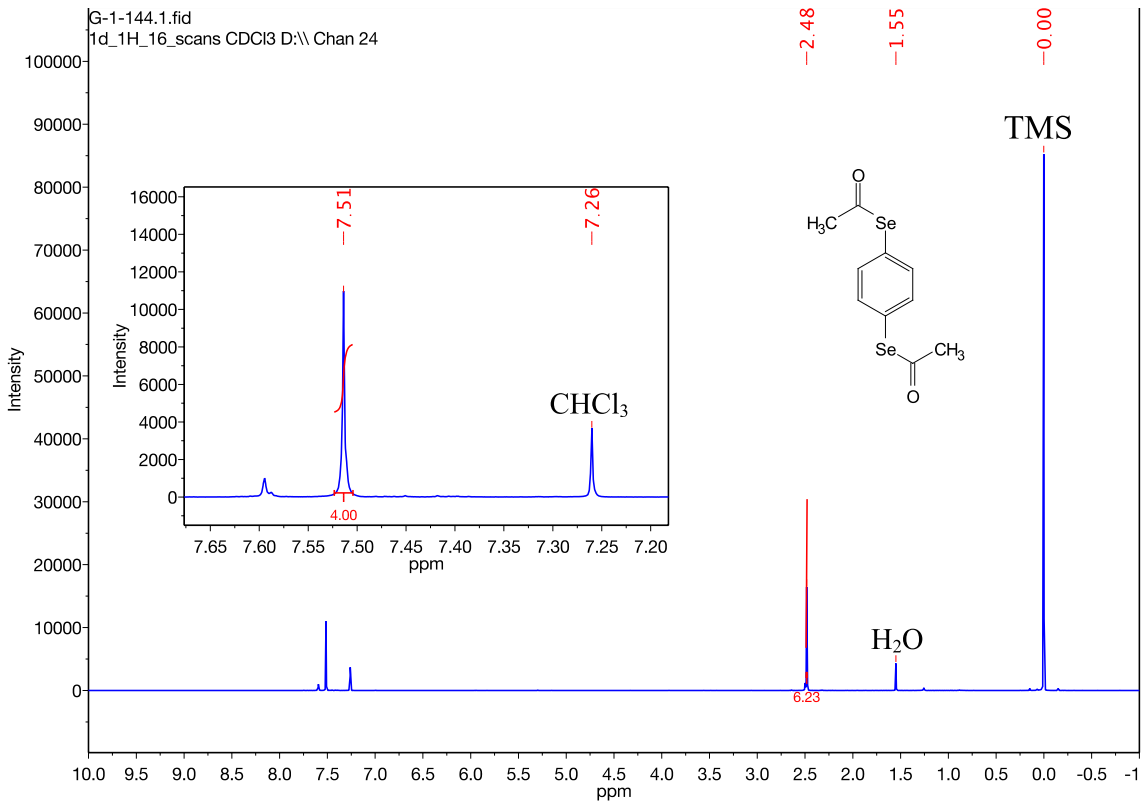


**Figure S6.** $^{1}$H NMR spectrum of 1,4-(diacetylseleno)benzene in $CDCl_3$.

## Thermogravimetric Analysis (TGA)

TGA curves were recorded under an air atmosphere, over the temperature range 25 - 500 °C, using a heating rate of 10 °C $min^{-1}$.

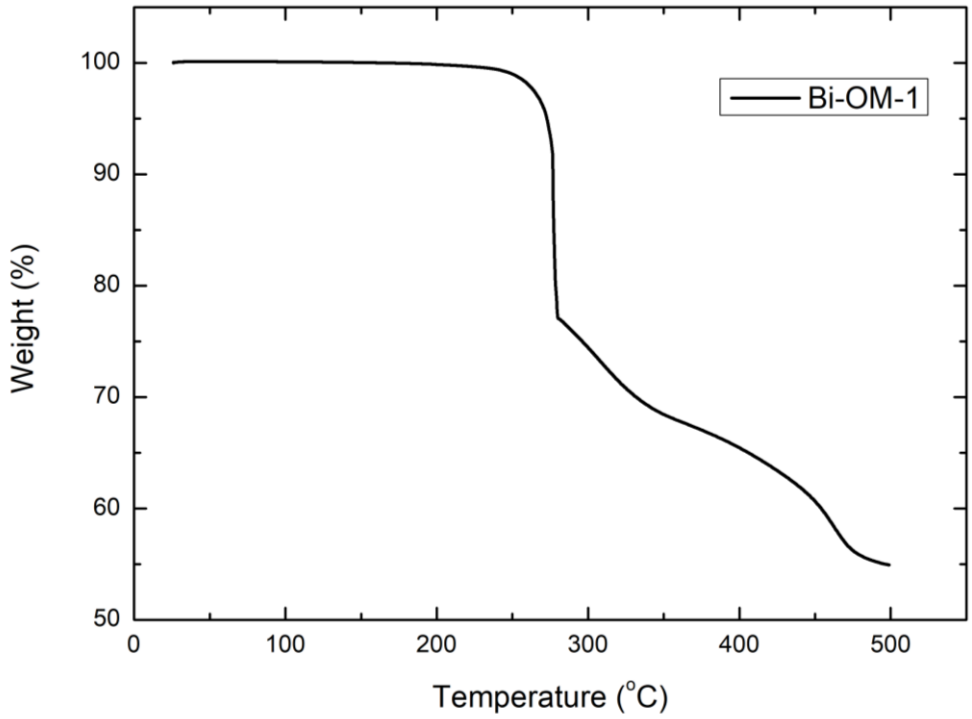


**Figure S7.** TGA curve of **Bi-OM-1**.

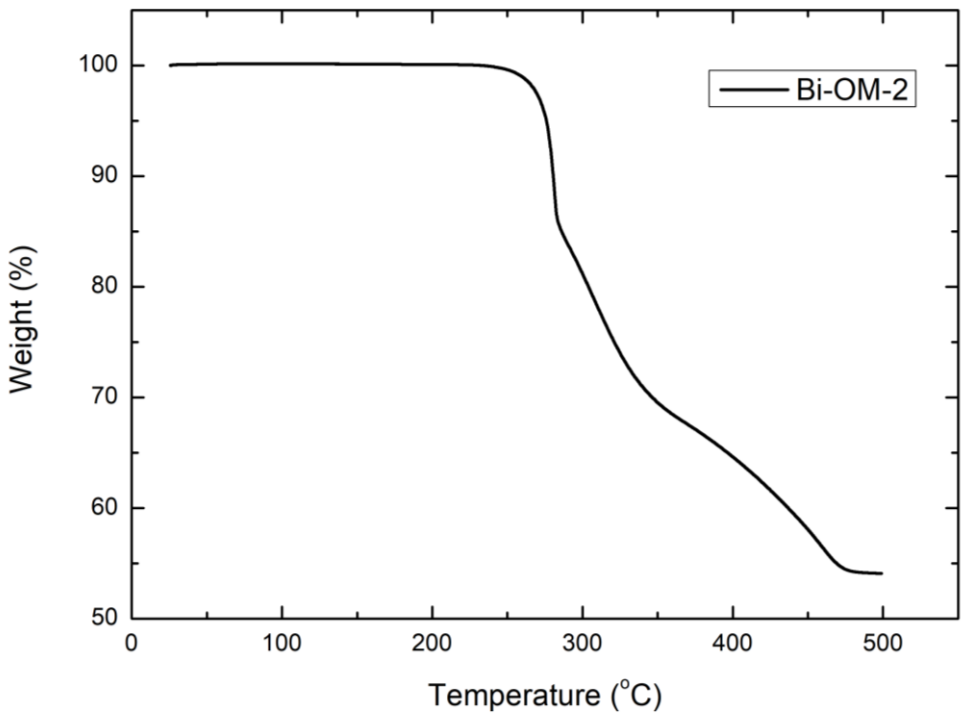


**Figure S8.** TGA curve of **Bi-OM-2**.

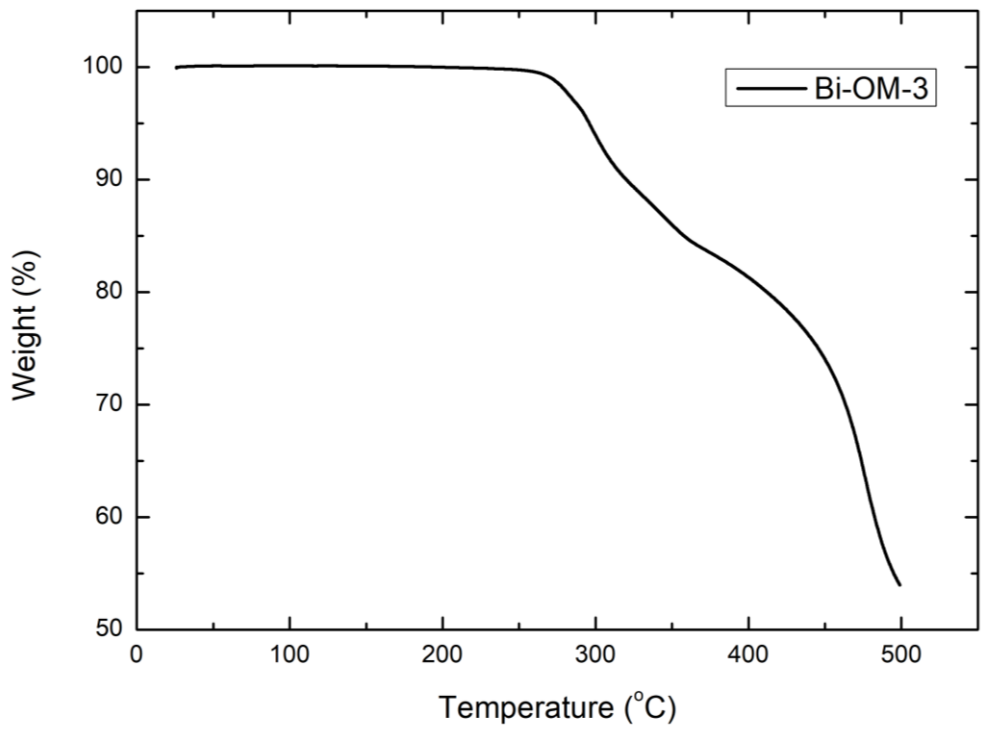


**Figure S9.** TGA curve of **Bi-OM-3**.

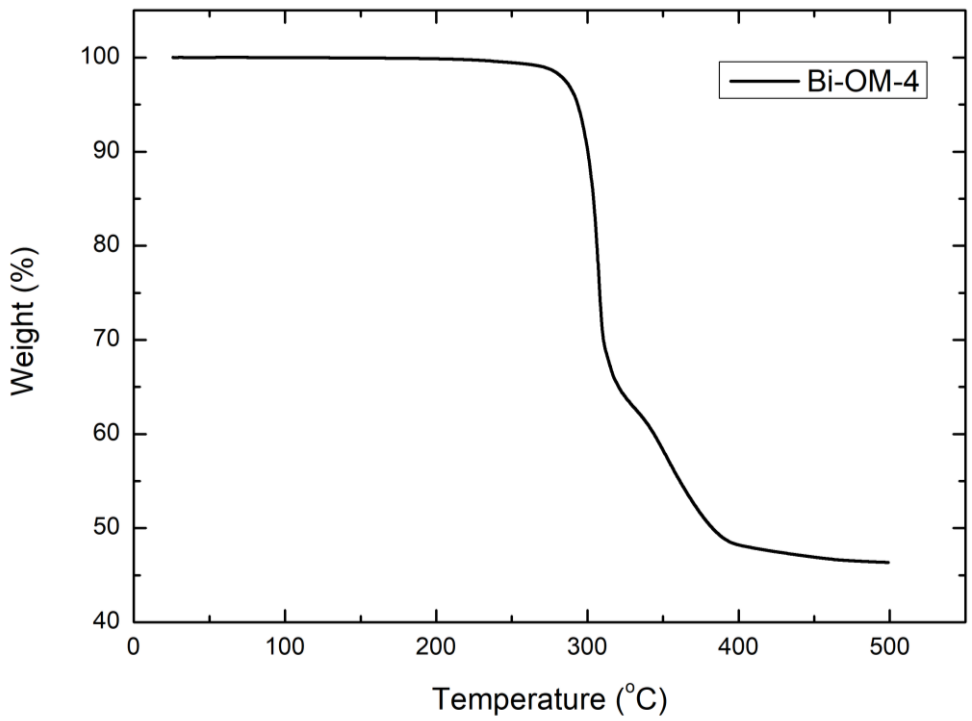


**Figure S10.** TGA curve of **Bi-OM-4**.

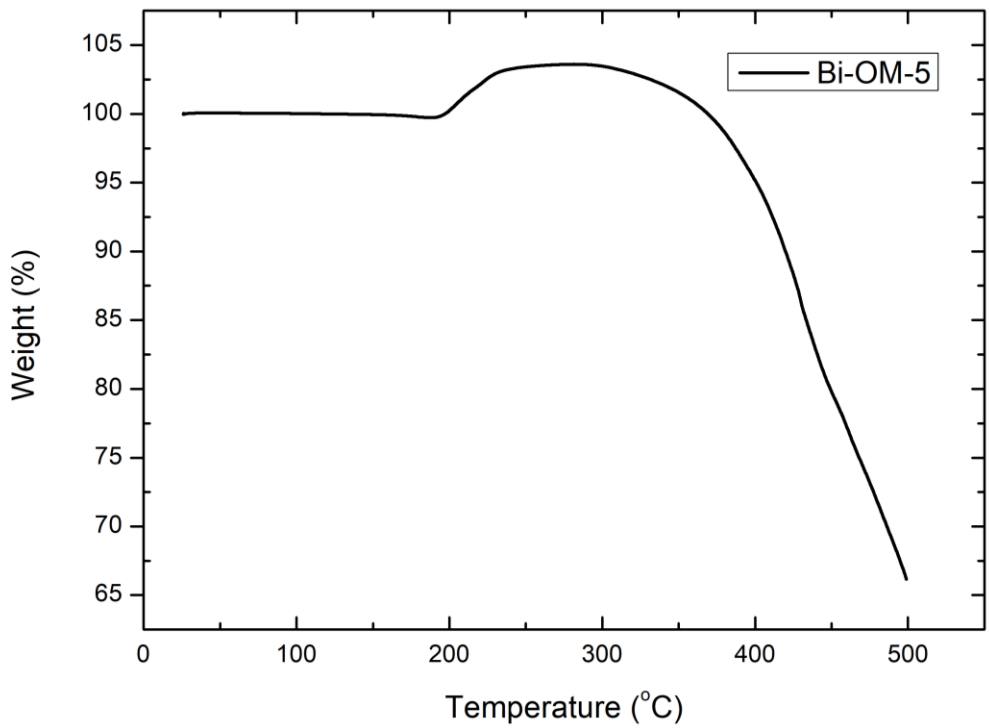


**Figure S11.** TGA curve of **Bi-OM-5**. (N. B. The initial weight increase at 200 °C suggests oxidation of Se centers prior to decomposition and subsequent mass loss at higher temperatures.)

## Energy-dispersive X-ray spectroscopy (EDS) Analysis

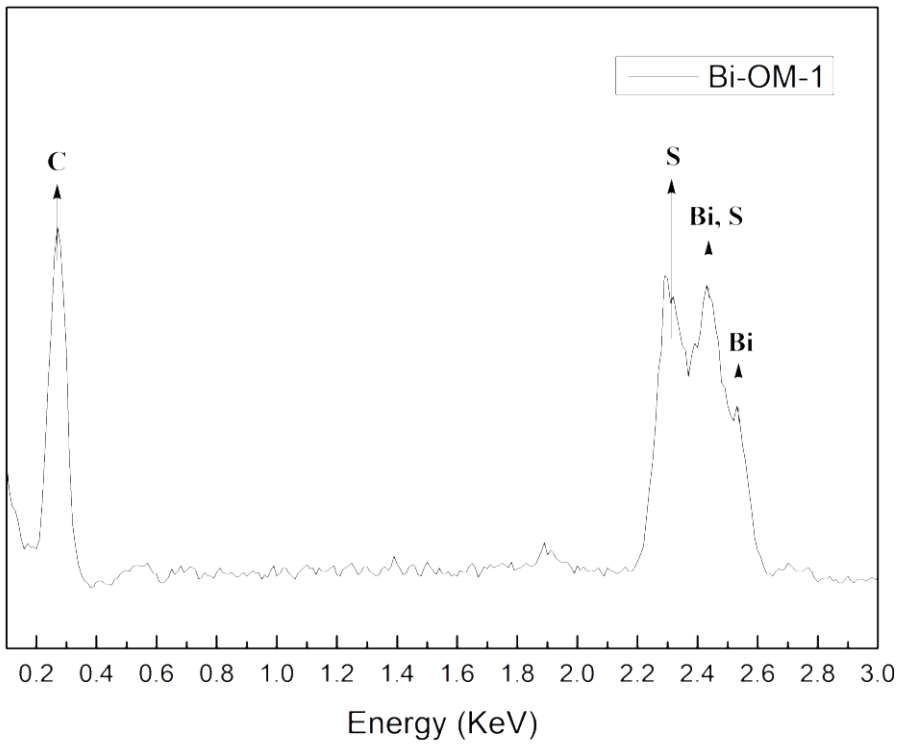


**Figure S12.** EDS spectrum of **Bi-OM-1**.

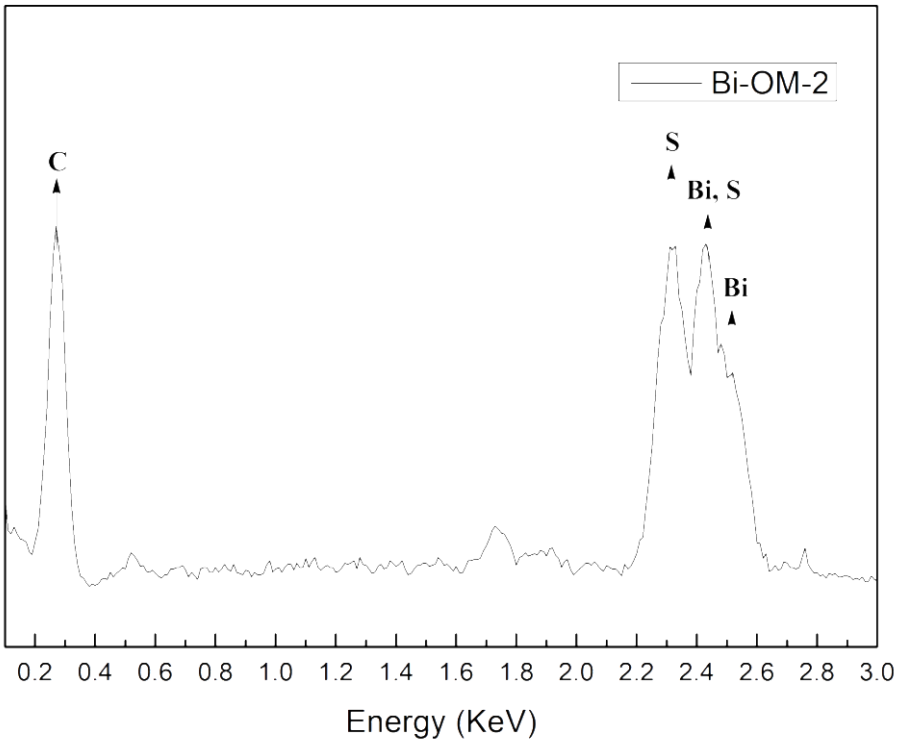


**Figure S13.** EDS spectrum of **Bi-OM-2**.

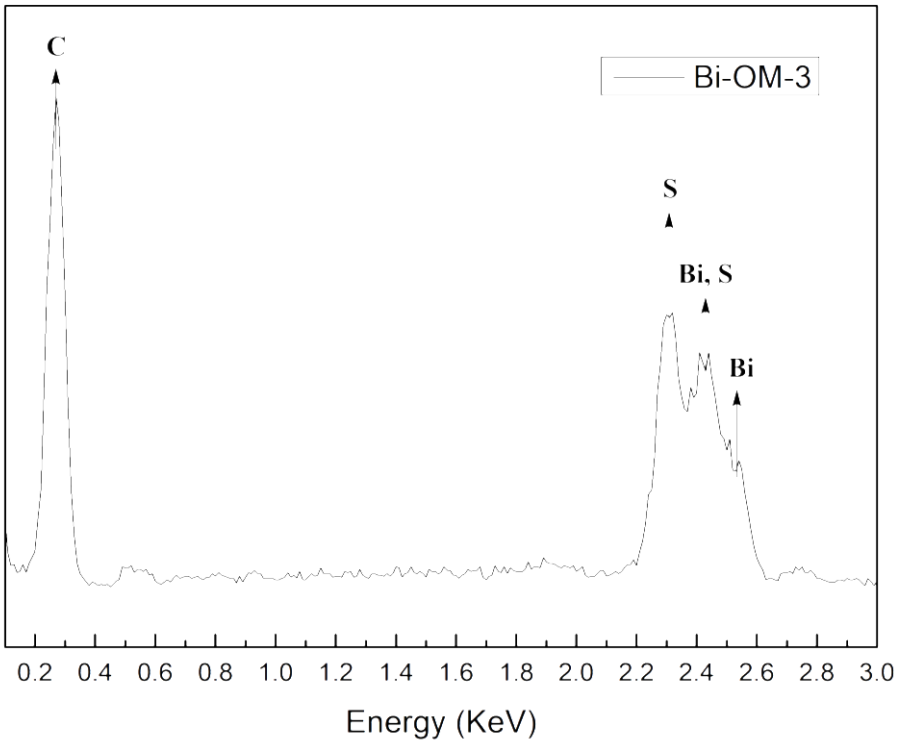


**Figure S14.** EDS spectrum of **Bi-OM-3**.

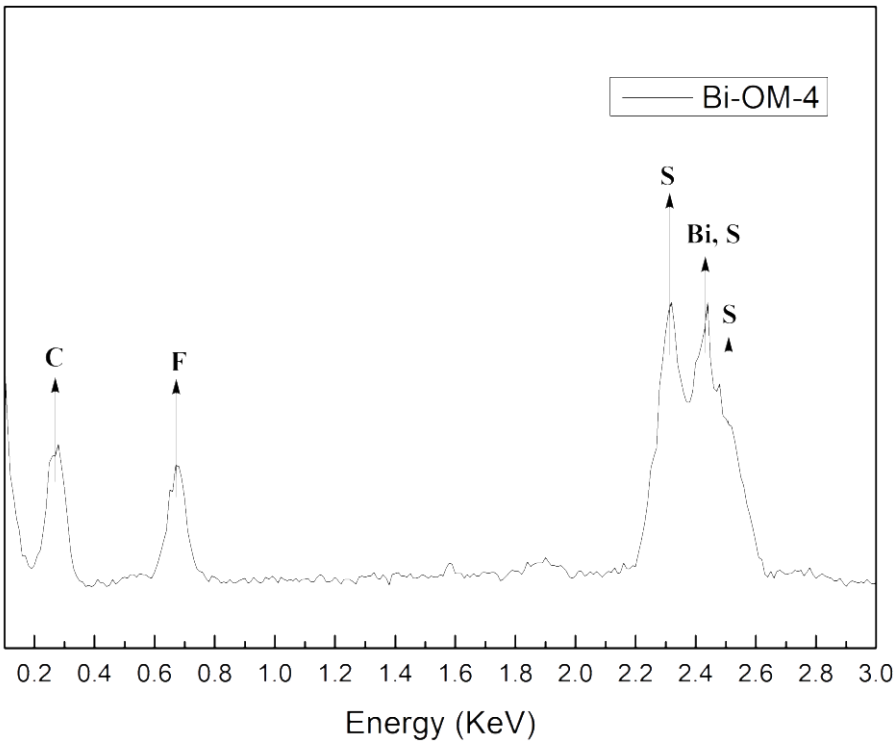


**Figure S15.** EDS spectrum of **Bi-OM-4**.

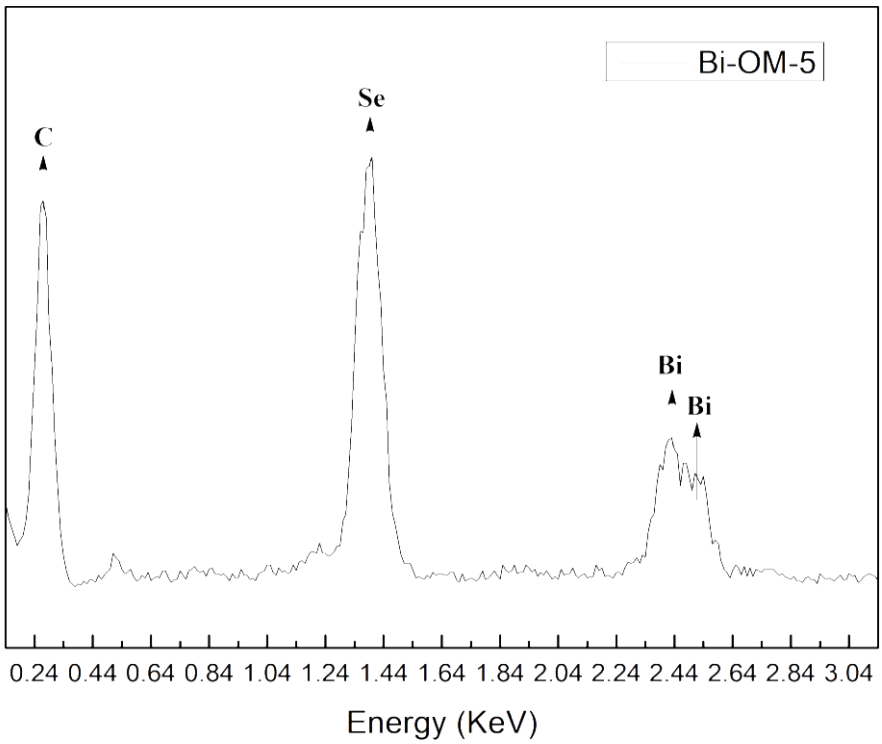


**Figure S16.** EDS spectrum of **Bi-OM-5**.

**Structural analysis.** Molecular modeling and Pawley refinement were carried out using Reflex plus module of Materials Studio 6.0. We performed Pawley refinements in the 2θ range of 2-80° to optimize unit-cell parameters, zero point, and background of Bi-OM-1 until the $R_{wp}$ value converged. The Pseudo-Voigt profile function was used for the whole profile fitting and Berrar-Baldinozzi function was used for asymmetry correction during the refinement processes. The final $R_{wp}$ and $R_p$ values were 6.90% and 5.09%, respectively. A simulated PXRD pattern was calculated from the refined unit cell and compared with the experimentally observed pattern, whereby good agreement was obtained.

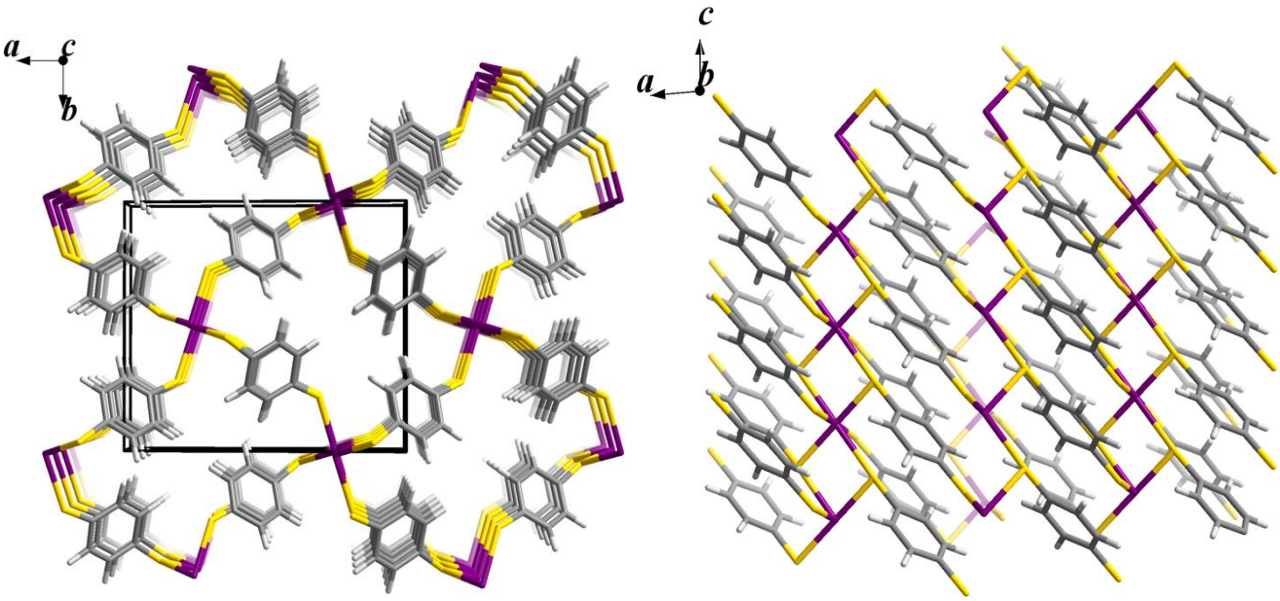


**Figure S17.** Simulated structure of Bi-OM-1 as generated by Materials Studio 6.0 (Accelrys) software.

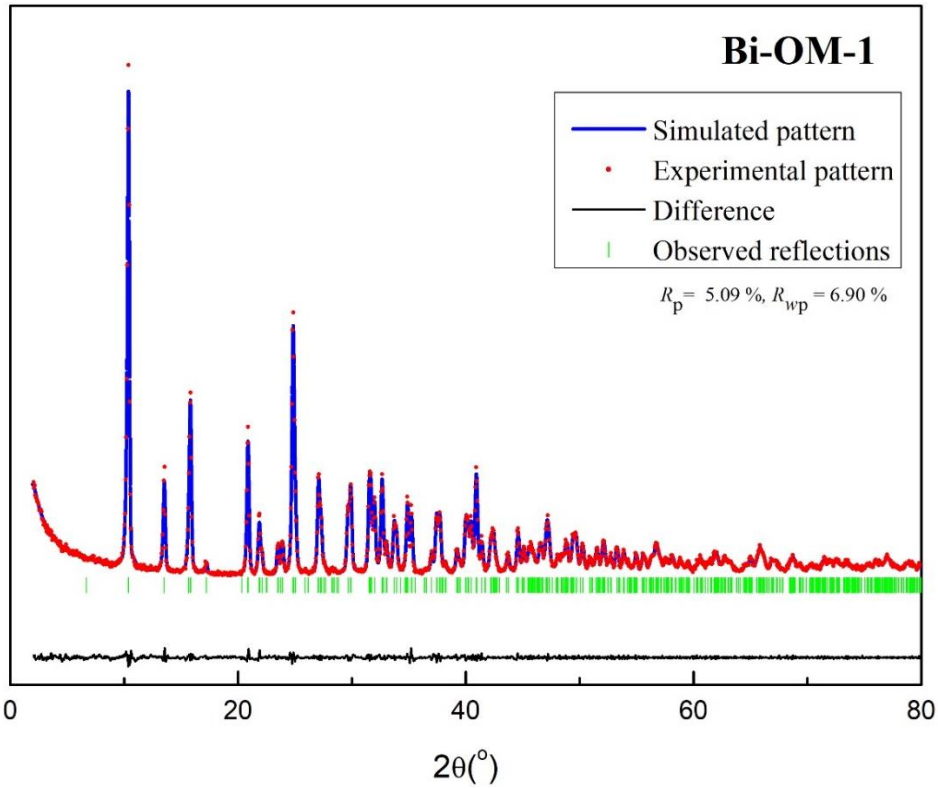


**Figure S18.** Simulated vs. experimental PXRD patterns of Bi-OM-1.

Unit cell parameters of Bi-OM-1

| Space Group | a (Å) | b (Å) | c (Å) | α (°) | β (°) | γ (°) | V(Å$^3$) |
|---|---|---|---|---|---|---|---|
| $P2_1$ | 13.101(4) | 11.160(3) | 4.027(1) | 90 | 95.269(3) | 90 | 586.3 |

Pawley refinements were also applied to the other four Bi-OMs materials using the same methods as the one employed for Bi-OM-1 due to the similarities in molecular structures of the five Bi-OMs materials. The simulated PXRD patterns of the other four Bi-OMs were also found to be in good agreement with their respective experimental observed patterns. These results are given below.

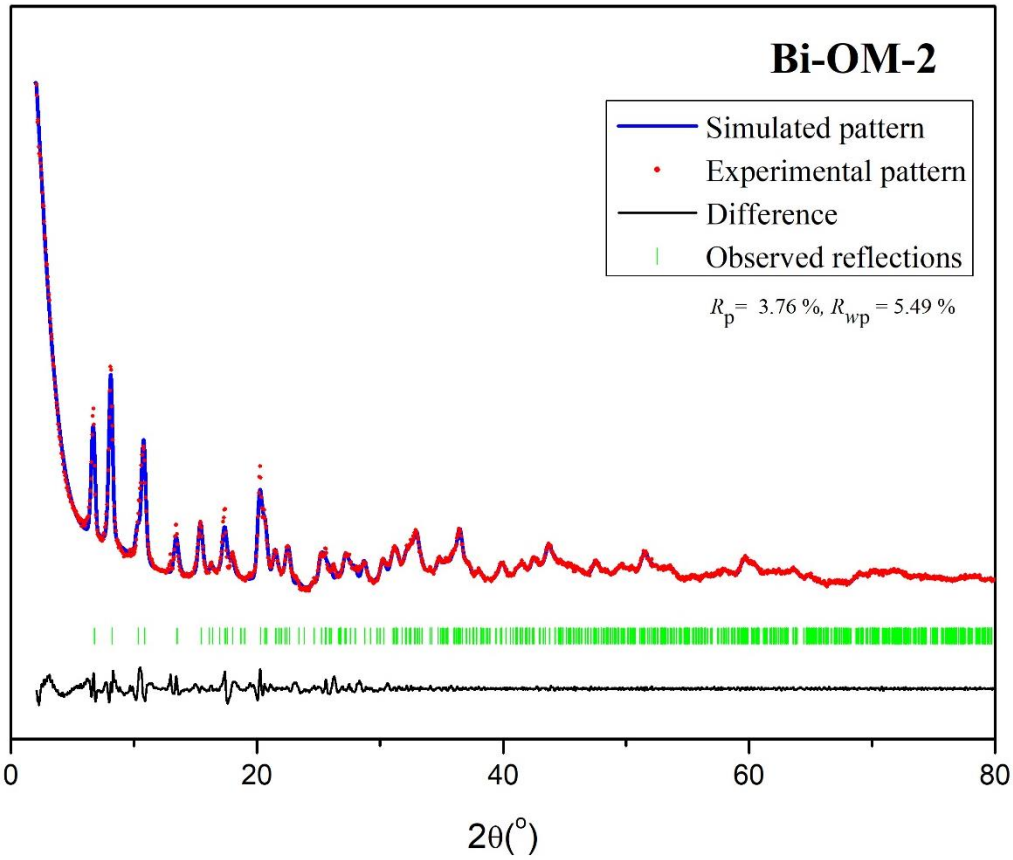


**Figure S19.** Simulated vs. experimental PXRD patterns of Bi-OM-2.

Unit cell parameters of Bi-OM-2

| Space Group | a (Å) | b (Å) | c (Å) | α (°) | β (°) | γ (°) | V(Å$^3$) |
|---|---|---|---|---|---|---|---|
| $P2_1$ | 13.178(11) | 5.719(4) | 10.870(9) | 90 | 92.697(10) | 90 | 818.3 |

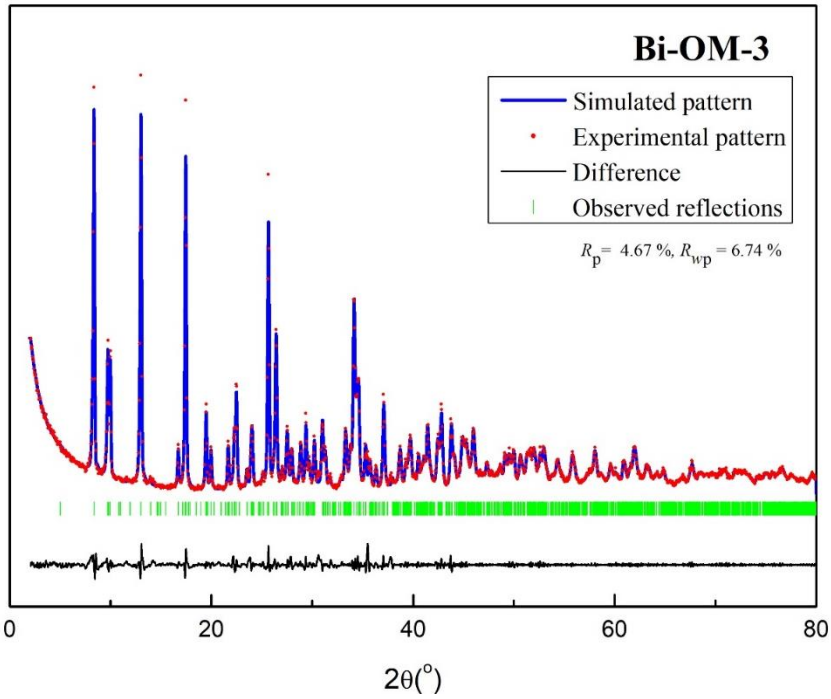


**Figure S20.** Simulated vs. experimental PXRD patterns of Bi-OM-3.

Unit cell parameters of Bi-OM-3

| Space Group | a (Å) | b (Å) | c (Å) | α (°) | β (°) | γ (°) | V(Å$^3$) |
|---|---|---|---|---|---|---|---|
| $P2_1$ | 11.025(3) | 17.658(5) | 9.404(3) | 90 | 107.119(2) | 90 | 1749.7 |

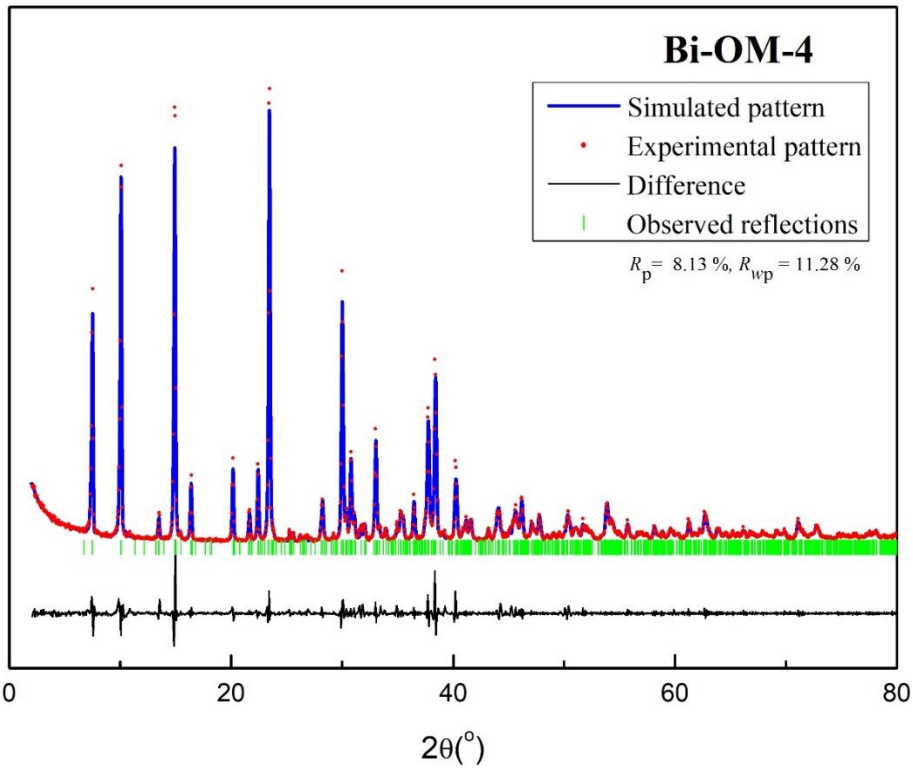


**Figure S21.** Simulated vs. experimental PXRD patterns of Bi-OM-4.

Unit cell parameters of Bi-OM-4

| Space Group | a (Å) | b (Å) | c (Å) | α (°) | β (°) | γ (°) | V(Å$^3$) |
|---|---|---|---|---|---|---|---|
| $P2_1$ | 12.054(3) | 13.140(4) | 7.991(2) | 90 | 102.508(2) | 90 | 1235.7 |

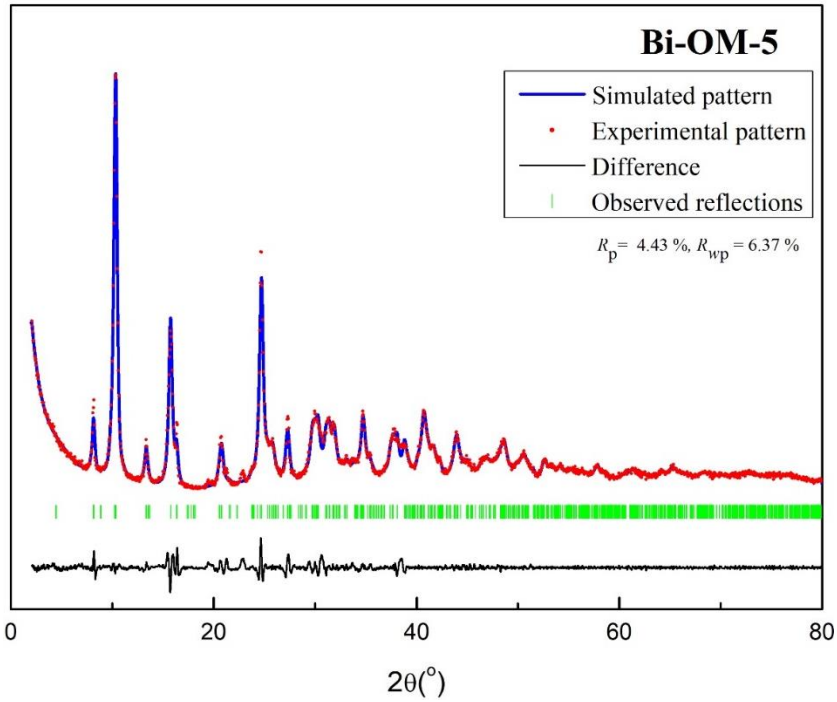


**Figure S22.** Simulated vs. experimental PXRD patterns of Bi-OM-5.

Unit cell parameters of Bi-OM-5

| Space Group | a (Å) | b (Å) | c (Å) | α (°) | β (°) | γ (°) | V(Å$^3$) |
|---|---|---|---|---|---|---|---|
| $P2_1$ | 25.943(24) | 3.717(4) | 11.240(2) | 90 | 129.962(2) | 90 | 830.8 |

**Porosimetry studies.** Surface area (BET) measurements indicated that our Bi-OM was of a nonporous nature with low surface area and small pore volumes (representative example shown below in Figure S18), which is commonly encountered with bismuth-containing network structures.[4] For example, bismuth-organic frameworks tend to adopt dense or layered nonporous structures due to the flexible coordination geometry and high coordination number of bismuth,[4] and its propensity to form secondary bonding interactions. These results further support multiple secondary soft-soft bonding interactions between Bi and S atoms within the network structure.

**Pore Volume**

t-Plot micropore volume: 0.004367 cm³/g

BJH Adsorption cumulative volume of pores between 1.7000 nm and 300.0000 nm width: 0.056100 cm³/g

BJH Desorption cumulative volume of pores between 1.7000 nm and 300.0000 nm width: 0.055515 cm³/g

**Pore Size**

BJH Adsorption average pore width (4V/A): 25.9132 nm

BJH Desorption average pore width (4V/A): 29.2444 nm

**Surface Area**

Single point surface area at p/p° = 0.300000000: 15.7197 m²/g

BET Surface Area: 18.2771 m²/g

t-Plot Micropore Area: 10.5868 m²/g

t-Plot external surface area: 7.6903 m²/g

BJH Adsorption cumulative surface area of pores between 1.7000 nm and 300.0000 nm width: 8.660 m²/g

BJH Desorption cumulative surface area of pores between 1.7000 nm and 300.0000 nm width: 7.5933 m²/g

**BET Report**

BET surface area: 18.2771 ± 0.3834 m²/g
Slope: 0.237073 ± 0.004960 g/cm³ STP
Y-intercept: 0.001071 ± 0.000595 g/cm³ STP
C: 222.449918
Qm: 4.1991 cm³/g STP
Correlation coefficient: 0.9993441
Molecular cross-sectional area: 0.1620 nm²

| Relative Pressure (p/p°) | Quantity Adsorbed (cm³/g STP) | 1/[Q(p°/p - 1)] |
|---|---|---|
| 0.064796762 | 4.1390 | 0.016740 |
| 0.073624605 | 4.2657 | 0.018631 |
| 0.107758768 | 4.6244 | 0.026116 |
| 0.141507815 | 4.8068 | 0.034292 |
| 0.175246780 | 4.9381 | 0.043030 |

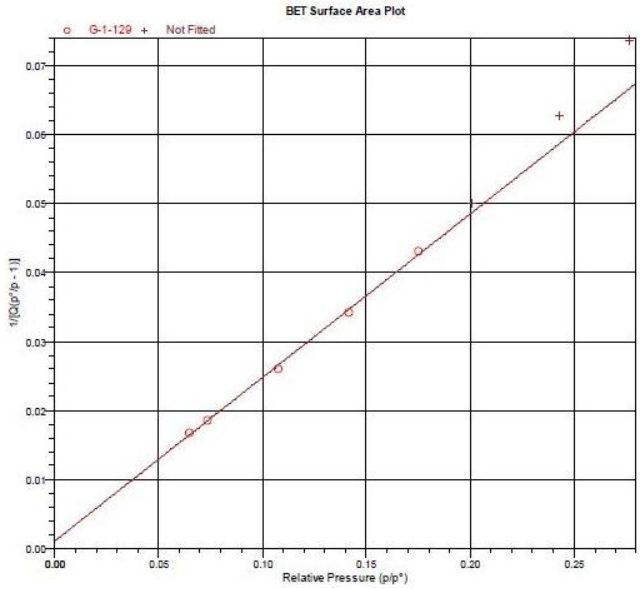


**Figure S23.** Brunauer-Emmett-Teller (BET) surface area and pore volume/size data for Bi-OM-1.

## References


(1) Roberson, A. P. M.; Burford, N.; McDonald, R.; Ferguson, M. J. Coordination complexes of $Ph_3Sb^{2+}$ and $Ph_3Bi^{2+}$: Beyond pnictonium cation. *Angew. Chem. Int. Ed.* **2014**, *53*, 3480-3483.

(2) Umemoto, T.; Garrick, L.; Saito, N. Discovery of practical production processes for arylsulfur pentafluorides and their higher homologues, bis- and tris(sulfur pentafluorides): Beginning of a new era of "super-trifluoromethyl" arene chemistry and its industry. *Beilstein J. Org. Chem*. **2012**, *8*, 461-471.

(3) Boer, B.; Meng, H.; Perepichka, D. F.; Zheng, J.; Frank, M. M.; Chabal, Y. J.; Bao, Z. Synthesis and characterization of conjugated mono- and dithiol oligomers and characterization of their self-assembled monolayers. *Langmuir* **2003**, *19*, 4272-4284.

(4) Inge, A. K.; Köppen, M.; Su, J.; Feyand, M.; Xu, H.; Zou, X.; O'Keeffe, M.; Stock, N. Unprecedented Topological Complexity in a Metal–Organic Framework Constructed from Simple Building Units. *J. Am. Chem. Soc.* **2016**, *138*, 1970–1976.